

Correlative Light-Electron Fractography of Interlaminar Fracture in a Carbon-Epoxy Composite

Luis Rogerio de O. Hein,^{*} and Kamila A. de Campos

Materials Imaging Lab, Department of Materials and Technology, Faculty of Engineering at Guaratinguetá, UNESP – Universidade Estadual Paulista, Av. Ariberto Pereira da Cunha 333, Guaratinguetá, SP 12516-410, Brazil

Abstract: This work evaluates the use of light microscopes (LMs) as a tool for interlaminar fracture of polymer composite investigation with the aid of correlative fractography. Correlative fractography consists of an association of the extended depth of focus (EDF) method, based on reflected LM, with scanning electron microscopy (SEM) to evaluate interlaminar fractures. The use of these combined techniques is exemplified here for the mode I fracture of carbon-epoxy plain-weave reinforced composite. The EDF-LM is a digital image-processing method that consists of the extraction of in-focus pixels for each x - y coordinate in an image from a stack of Z -ordered digital pictures from an LM, resulting in a fully focused picture and a height elevation map for each stack. SEM is the most used tool for the identification of fracture mechanisms in a qualitative approach, with the combined advantages of a large focus depth and fine lateral resolution. However, LMs, with EDF software, may bypass the restriction on focus depth and present enough lateral resolution at low magnification. Finally, correlative fractography can provide the general comprehension of fracture processes, with the benefits of the association of different resolution scales and contrast modes.

Key words: composites, correlative microscopy, light microscopy, electron microscopy, fractography

INTRODUCTION

There are many representative publications on the fractography of long fiber polymer composites. Certainly, most composite researchers found inspiration in the series of articles published by Purslow in the 1980s (Purslow, 1981, 1986, 1987a, 1987b, 1988a, 1988b; Potter & Purslow, 1983; Purslow & Potter, 1984), or in the books authored and co-authored by Hull in 1990s (Hull & Clyne, 1996; Hull, 1999), and, more recently, in Greenhalgh's book (Greenhalgh, 2009).

In general, the literature on fracture analysis of polymer composites recommends the use of scanning electron microscopy (SEM) owing to its intrinsic advantages: large depth of field and fine lateral resolution. Authors generally minimize SEM limitations relative to specimen handling: costly operation, vacuum degradation, electron beam-induced damage, charging effects, sputter-coating artifacts, and others. In fact, SEM produces sharp and representative images of fracture surfaces, especially when using the secondary electron signal. Some alternatives reduce SEM limitations, such as the use of low-voltage or variable pressure modes for imaging (Sawyer et al., 2008), which permit avoidance of most of the restrictions of conventional SEM (high voltage at high vacuum of metal-coated samples): charging effects, need for sputter coating or carbon evaporation, and beam damage or large vacuum degradation. In the current generation of signal detectors for variable pressure/environmental SEMs, it is even possible to combine low beam voltage with low vacuum

modes (Hein et al., 2012a), despite the electron gas-scattering limitation, to produce images at high enough magnification for the analysis of fracture mechanisms.

In contrast, light microscopes (LMs) have not been used extensively in failure analysis of polymer composites. Purslow (1984) presented a “successful failure analysis of an aerospace structural element using low-power optical microscopy alone,” finding “the initial cause of ultimate failure of a typical aerospace structural element.” Of course, it was possible for interlaminar fracture, less affected by the restriction of in-focus depth than other fracture modes, such as intralaminar and translaminar ones. Greenhalgh (2009) undervalued LM, generalizing “compound microscopy is of less importance for fractography of polymer composites,” reinforcing that the focus depth and vibration issues could affect image quality in light compound and stereo microscopes.

Interlaminar fracture can be observed with conventional LMs with an extended depth of focus (EDF) software tool. It consists of the acquisition of a sequence of digital images with progressive focusing with a constant step in elevation, and taking the best-focused pixels for each x - y position throughout the entire stack to construct a focused picture to provide a reliable elevation map. A myriad of image-processing algorithms for EDF reconstruction is available today, including methods based on derivative and variance convolution filters in space domain, wavelets, and other frequency domain operators (Valdecasas et al., 2001; Forster et al., 2004). EDF solutions, based on conventional LMs, introduce quantitative topographic information for failure investigations at a considerably lower cost than confocal

scanning microscopy, covering larger and deeper areas than the atomic force microscopy, and without the limitations observed in shape from shading or stereo reconstruction methods offered for SEMs (Paluszyński & Słótko, 2009). In optical microscopy, the lateral resolution remains a limiting issue, but the analyst gains two important tools such as elevation maps and color contrast.

Finally, the correlative light-electron fractography method (Hein et al., 2013a, 2013b) presented here combines, pixel by pixel, the quantitative topography and contrast information provided by LMs to the fine lateral resolution from SEMs. It should permit translation of well-known fracture features from SEM images to those with LMs, paving the path for new development for fracture investigation of polymer composites. This paper presents some examples of this approach with comments about the aspects of fracture features described by each microscopy technique.

MATERIALS AND METHODS

Specimens and Testing

Specimens came from laminated plates of carbon-epoxy composite, produced with pre-impregnated plain weaves (Tencate BT-50E-1, Koninklijke Tencate nv, Nijverdal, The Netherlands) by pressing with an aluminum foil inserted at the middle plane of the laminate to generate the starter crack.

Double cantilever beam (DCB) tests were conducted according to ASTM D5528-07 (ASTM D5528-13, 2013) to determine the mode I interlaminar fracture toughness (G_I), using a Shimadzu AG-X machine (Shimadzu Corporation, Kyoto, Japan) at 2.0 mm/min displacement rate.

Microscopy Techniques

Fractured DCB specimens were fixed on the CorrMic A sample holder (Carl Zeiss Microimaging GmbH, Göttingen, Germany) of the Zeiss “Shuttle & Find” hardware (Carl Zeiss Microimaging GmbH) and software solution for correlative microscopy, mounted on a Zeiss AxioImager Z2m motorized LM (Carl Zeiss Microimaging GmbH). The spatial (x, y) reference system was calibrated according to marks on the sample holder, using the Shuttle & Find plugin for Zeiss AxioVision 4.8. Image stacks were pictured with a set of objective lenses (a 20×/0.4 EC Epiplan HD/DIC (Carl Zeiss Microimaging GmbH), a 50×/0.55 LD EC Epiplan Neofluar HD DIC, and a 100×/0.75 LD EC Epiplan Neofluar HD DIC), under bright field (BF), dark field (DF), circular polarization (CP), and linear polarization (LP) contrast modes for the same spatial (x, y, z) coordinates on the sample. The “Topography” plugin for Zeiss AxioVision 4.8 (Carl Zeiss Microimaging GmbH) was set to obtain the image stacks with constant Z intervals, with a 10 nm resolution, according to the objective lenses: 1.00 μm for 20×, 0.5 μm for 50×, and 0.25 μm for the 100×. The EDF reconstructions of LM image stacks were processed under the Topography module for Zeiss AxioVision 4.8 to provide focused LM images for the correlation with

corresponding SEM images. An alternative for EDF reconstruction is the myriad of EDF plugins available for National Institutes of Health (NIH) ImageJ. Some of those plugins were evaluated in an earlier paper by the present authors (Hein et al., 2012b). These provide analysts with free reliable software options to reproduce these results.

After this step, the sample holder was mounted on the SEM, a Zeiss EVO LS-15 (Carl Zeiss SMT Ltd, Cambridge, UK). The SEM stage was then calibrated with the Zeiss AxioVision 4.8 “Shuttle & Find” module by finding the reference marks, at low-voltage mode. The optimum level of beam energy (0.9 keV in this case) was defined according to the procedure developed by Hein et al. (2013c) for the carbon-epoxy composite finding the optimum imaging condition for the range from 0.7 to 1.2 keV, as the boundary values for E_2 crossover secondary electron energies. Long fiber carbon-epoxy composites have heterogeneous properties of electric conductivity, where the conductive carbon fibers redistribute the charge carriers, whereas the insulator character of the epoxy resin sustains the charge imbalance, acting as a floating conductor (Craven et al., 2002).

Finally, the image files corresponding to the focused pictures for each LM stack were loaded into the Zeiss AxioVision program, driving the SEM stage to almost the same (x, y) fields pictured with the LM. These images were then aligned with corresponding pictures from LM using the Shuttle & Find plugin for Zeiss AxioVision 4.8.

Other freeware tools for NIH ImageJ public domain software (Rasband, 2015) for image processing and analysis were also useful plugins for the analysis of image alignment: the Hajime Hirase’s “iMorph” (<http://rsbweb.nih.gov/ij/plugins/morph.html>) and the Interactive 3-D Surface Plot (<http://rsbweb.nih.gov/ij/plugins/surface-plot-3d.html>) by Kai Uwe Barthel. Matched correlative images had the contrast enhanced under NIH ImageJ.

For focused LM and SEM pictures, the image lateral resolution was measured by the SMART-J plugin designed by Dr. David C. Joy (2002) based on measurements on Fourier domain, after fast Fourier transform. All the measurements were done for 8-bit grayscale images, converted from RGB 24-bit color space with the NIH ImageJ program.

RESULTS AND DISCUSSION

At low magnification, LM can reveal the general aspects of interlaminar composites fracture. Using the 20× objective lens of the LM, the most impressive pictures were collected with BF or DF illumination modes, with a tendency to brightness saturation in the last one (Figs. 1a, 1b). At this magnification level, BF and DF images present lateral resolution comparable with that provided by SEM (Table 1), but some fibers under the surface are revealed owing to the transparency of epoxy resin. Under LP or CP light-contrast modes (Figs. 1c, 1d), the lateral resolution is larger (Table 1), not revealing the finest details of resin fracture, but the information is more restricted to the surface than for BF

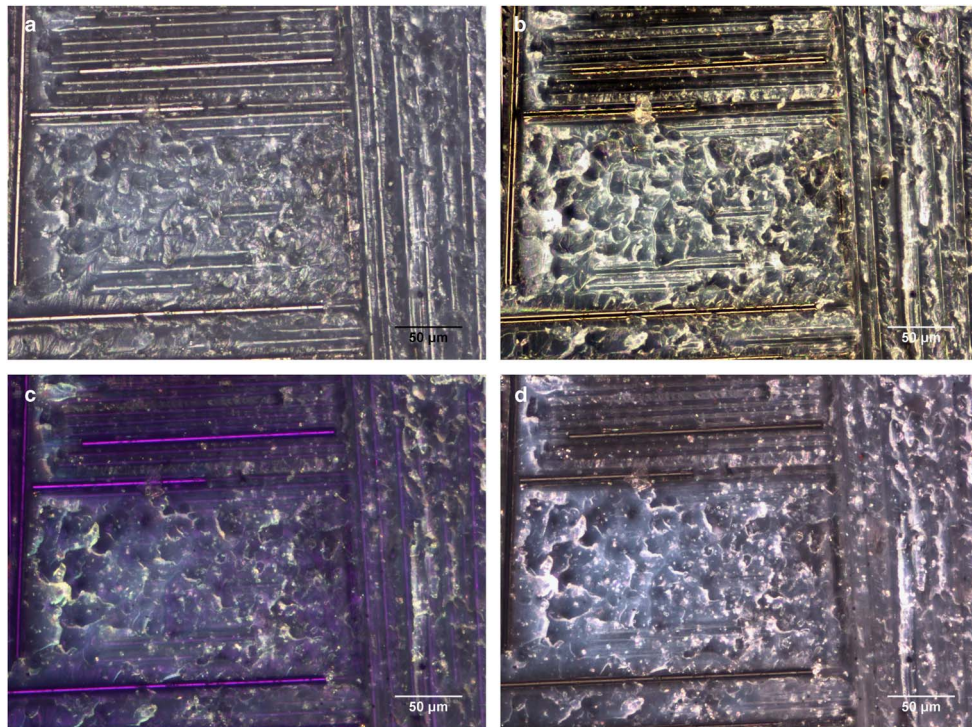


Figure 1. Extended depth of focus reconstructed fractographs for the light microscope with 20× objective lens at different illumination or contrast modes. **a:** Bright field; **(b)** dark field; **(c)** linear polarization; **(d)** circular polarization.

and DF modes. The corresponding height map reveals that the fibers anchor the resin deformation, as expected, but the intensity of this plastic deformation is larger between west-oriented fibers than for warp ones (Figs. 2a, 2b). The matching of LP LM images (Fig. 3a) with corresponding SEM secondary electron images (Fig. 3b) is presented in Figure 3c. In Figure 3c, color fringes are observed at the final edges of more intensively deformed scarps or textured microflow, and are indicative of resin ductility behavior. Scarps and textured microflow are easily recognized from SEM images (Fig. 3b), but the LM images (Fig. 3b) contributed with color fringes at resin regions, also coloring the fibers.

LM images acquired with the 50× objective lens (Fig. 4) provide a more detailed description of the fracture features than those presented in Figure 1, but the transparency effect of the epoxy matrix is strongly reduced under BF illumination (Fig. 4a). From Table 2, the lateral resolution of

CP-focused image (Fig. 4b) is still worse (394 nm) than that verified for the BF reconstructed one (388 nm), but the values are quite near each other, being more distant than the 318 nm of lateral resolution for the SEM corresponding image (Fig. 4c). In another way, fractographic features as textured microflow and scarps are more evident on the BF image than for the CP one, which has higher contrast in resin areas, evidencing the deformation issue.

Furthermore, the corresponding height maps aid analysis of the crack growth direction based on scarp relief, without the need to tilt the sample in the SEM chamber, by observing the behavior of a three-dimensional (3D) surface plot. Figures 5a and 5b is an example, presenting plots for SEM- and BF-focused images superimposed on 3D maps, enhancing the visibility of scarps and textured microflow, which grows according to the direction of the arrows. From the matched images, the correlative information gains relevance:

- SEM and BF LM: for Figures 6a to 6c, horizontal lines in the SEM image (Fig. 6a), which could be interpreted as scanning failure due to localized charging, are justified by the presence of subsurface fibers, revealed in the BF LM image (Fig. 6b) and related to the interface adhesion, which is emphasized on exposed fibers in correlated image by the contrast of adhered resin scarps (Fig. 6c).
- SEM and CP LM: for Figures 6d to 6f, brighter edges on CP images (Fig. 6e) are related only to resin, evidencing some fiber debris that is not highlighted in the SEM secondary electron images (Fig. 6d), as became clear in the correlated image (Fig. 6f).

Table 1. Comparison of Resolution Among Reconstructed Light Microscopic (LM) Pictures and Scanning Electron Microscopic (SEM) Image at 20× Objective Lens Magnification Level.

Images	Resolution (nm)	Pixel Size (nm)
LM—linear polarization	815	170
LM—bright field	596	170
LM—dark field	537	170
LM—circular polarization	718	170
SEM—secondary electrons detector at 0.9 keV	574	170

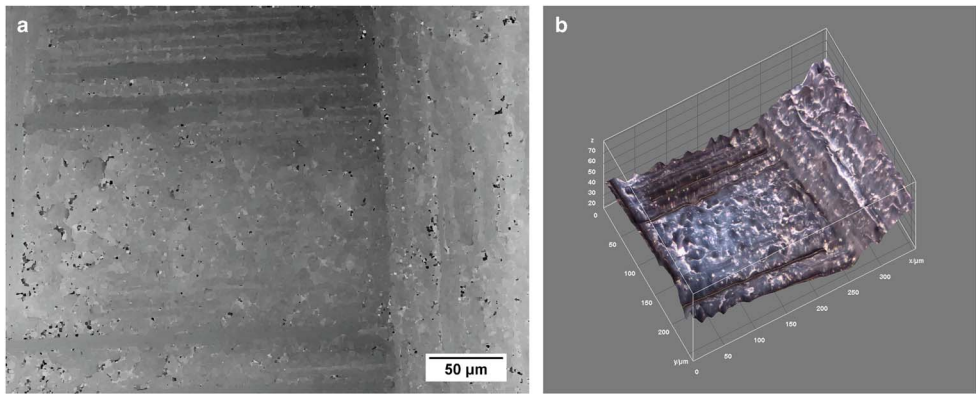


Figure 2. Example of corresponding height map of the extended depth of focus reconstruction from a light microscope stack under circular polarization contrast mode using the 20× objective lens. **a:** Height map; **(b)** three-dimensional surface plot of height map filled by the image in Figure 1d (circular polarization).

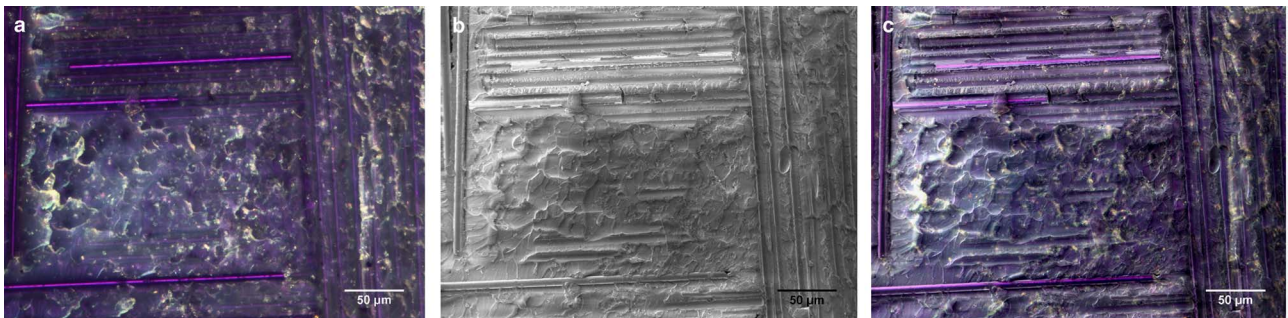


Figure 3. Example of correlative fractography with 20× objective lens. **a:** Extended depth of focus reconstructed image for linear polarization; **(b)** corresponding scanning electron microscopic (SEM) image with secondary electron detector; **(c)** matched image, combining information from light microscope and SEM.

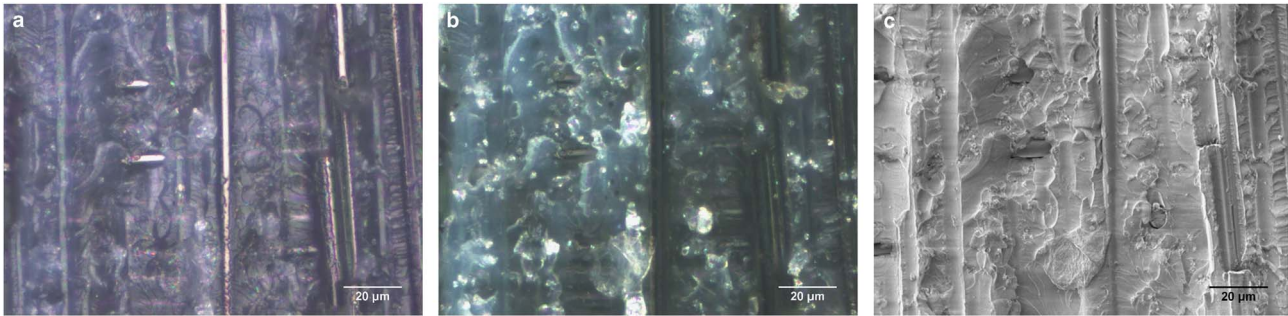


Figure 4. Extended depth of focus reconstructed light microscopic images with 50× objective lens. **a:** Bright field; **(b)** circular polarization; **(c)** corresponding scanning electron microscopic image using secondary electron detector.

c. Both correlative LM-SEM images clearly evidenced the interfacial anchorage of resin on fibers, promoting better distinction among the fiber imprints and those fibers covered by resin. The contrast also favored the comprehension of fracture topography, especially in understanding scarp behavior.

Using the 100× objective lens, LP (Fig. 7a) does not provide sharp details (333 nm of lateral resolution, see Table 3), but the color contrast discriminates the features, enhancing the resin scarps adhered to exposed fibers, and,

Table 2. Comparison of Resolution Among Reconstructed Light Microscopic (LM) Pictures and Scanning Electron Microscopic (SEM) Image at 50× Objective Lens Magnification Level.		
Images	Resolution (nm)	Pixel Size (nm)
LM—bright field	388	69
LM—circular polarization	394	69
SEM—secondary electrons detector at 0.9 keV	318	69

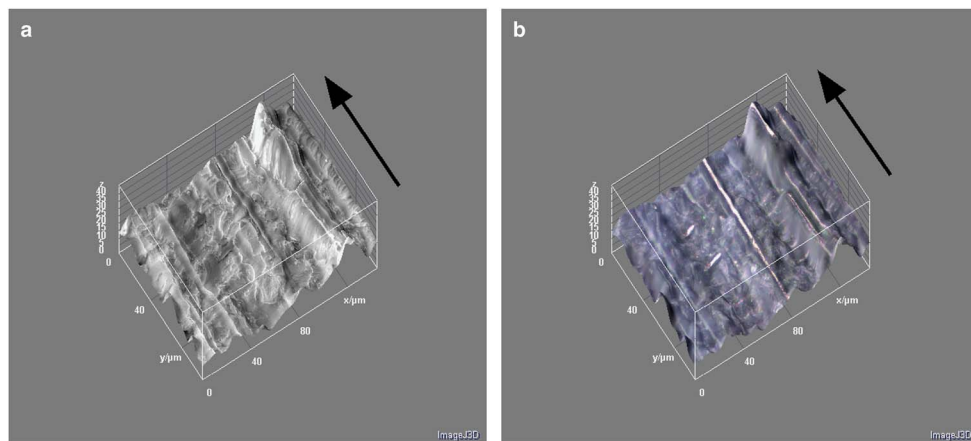


Figure 5. Three-dimensional surface plots filled with corresponding images to identify the crack growth direction (arrows). **a:** Scanning electron microscopic image; **(b)** bright-field light microscopic image.

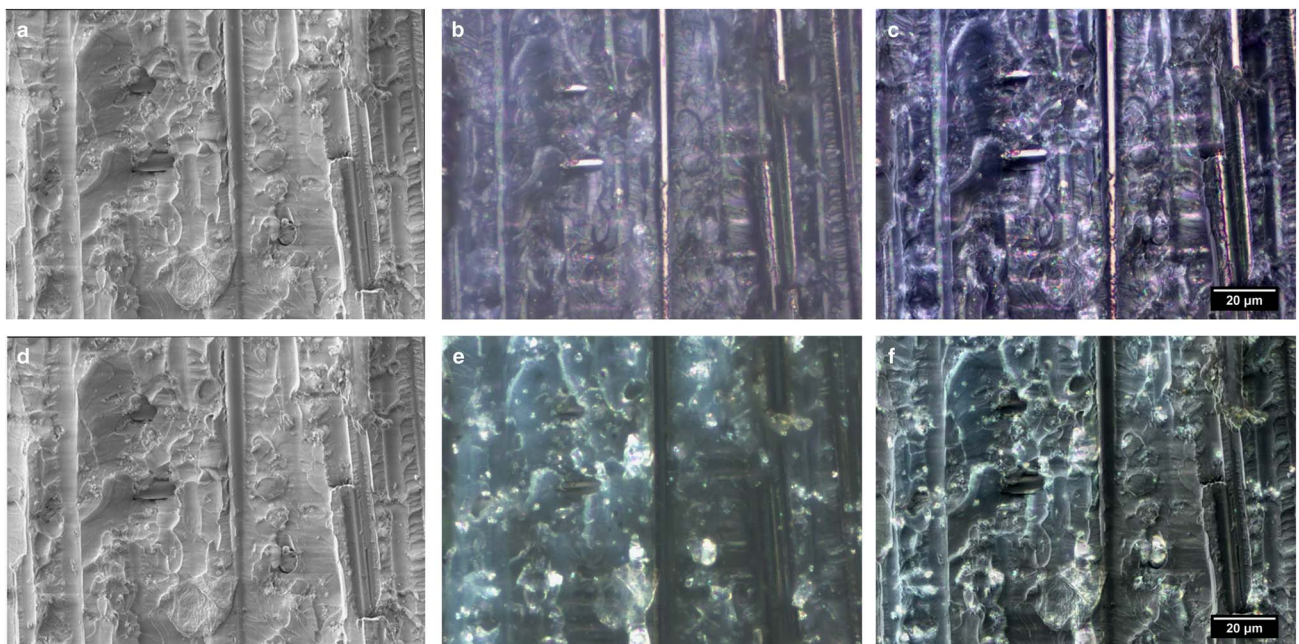


Figure 6. Correlative fractography with 50× objective lens. **a:** Scanning electron microscopic (SEM) image, displaced for matching; **(b)** light microscopic bright-field image; **(c)** correlative SEM-LM bright-field image; **(d)** matched SEM image; **(e)** LM circular polarization; **(f)** correlative SEM-LM picture.



Figure 7. Images for 100× objective lens magnification. **a:** Light microscopic (LM) linear polarization; **(b)** LM bright field; **(c)** scanning electron microscope.

Table 3. Comparison of Resolution Among Reconstructed Light Microscopic (LM) Pictures and Scanning Electron Microscopic (SEM) Image at 100× Objective Lens Magnification Level.

Images	Resolution (nm)	Pixel Size (nm)
LM—linear polarization	333	34
LM—bright field	290	34
SEM—secondary electrons detector at 0.9 keV	200	34

furthermore, providing a qualitative relationship between scarp brightness and local strain level. Otherwise, the BF image presents sharp boundaries and good color contrast, with a fine description of fracture features (Fig. 7b), such as scarps, textured microflow, and riverlines at 290 nm of lateral resolution. It is equivalent to information content in SEM images (Fig. 7c), despite the best lateral resolution in secondary electron images (200 nm). Correlative LM-SEM images just complete the information from the SEM images; however, the contrast is enhanced for SEM and BF or SEM and LP matched pictures (Figs. 8a, 8b). Again, 3D views of height maps with matched LM or SEM images provide the

right information about crack growth direction based on scarp behavior (Figs. 9a–9c).

CONCLUSION

The correlative light-electron fractography technique demonstrates how useful the LM can be for interlaminar fracture analysis in composites. It helps in the “translation” from the culture based on SEM fractography to interpret the fracture features in reconstructed pictures from LM. For these focused reconstructed LM images, the EDF algorithms can handle the restriction on focus depth in LM, whereas the lateral resolution is reasonably sufficient to study fractographic aspects at the magnification range used in most failure investigations. EDF height maps provide quantitative information about surface relief, being useful to determine crack propagation direction without the need of sample tilting into the SEM chamber.

The focus depth of LMs remains a limitation in the case of translaminar fracture, where aspects as pullouts and deep holes cannot be reconstructed by the EDF method. SEM imaging can deal with large depth transitions preserving fine lateral resolution, but the costs of ownership and maintenance for SEMs are higher than for an LM. In addition,

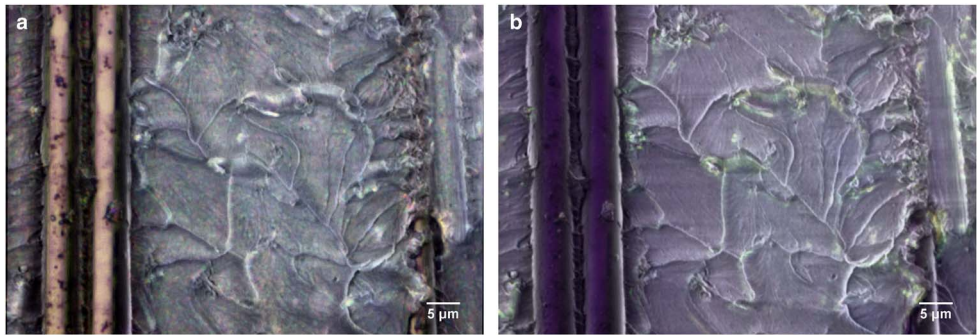


Figure 8. Correlative light microscope scanning electron microscope (LM-SEM) fractography at 100× objective lens magnification level. **a:** SEM and LM bright-field matched image; **(b)** SEM and LM linear polarization.

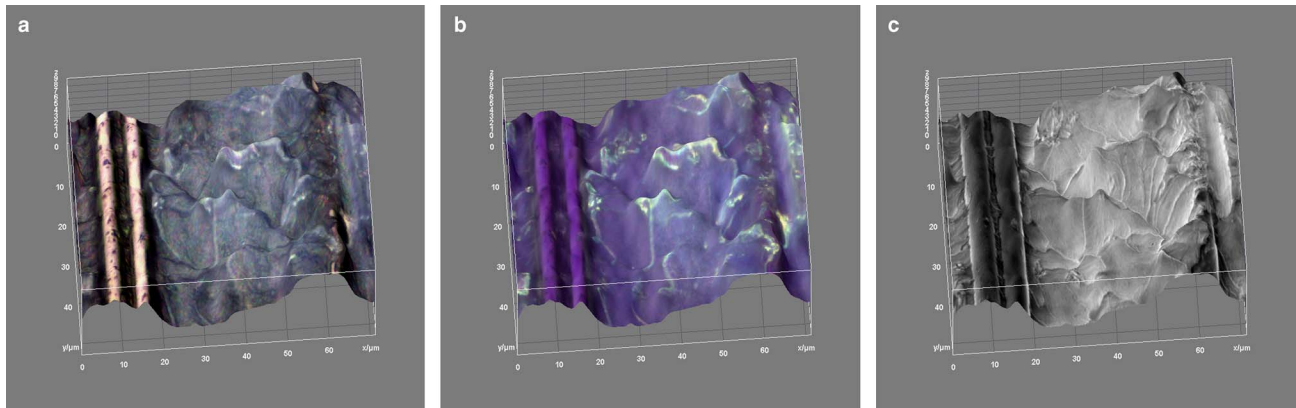


Figure 9. Three-dimensional surface plots from elevation maps with overlaid images. **a:** Light microscopic (LM) bright field; **(b)** LM linear polarization; **(c)** scanning electron microscope.

there are almost no restrictions about size, surface preparation, or degradation in handling specimens for LM, instead of the limitations in an SEM imposed by chamber size, vacuum needs, conductivity, and electron beam damage.

Finally, with many color-contrast choices in LM that are not present in grayscale SEM images, the analyst has an unexplored set of information to improve fracture investigations in composite materials.

ACKNOWLEDGMENTS

The authors are grateful to Dr. David C. Joy, from the University of Tennessee and Oak Ridge National Laboratory, who offered his quite useful SMART-J plugin for NIH ImageJ. Acknowledgments are also due to the authors, and their institutions, for the ImageJ plugins used in this work, and to Dr. Wayne Rasband, from the US National Institute of Mental Health (Bethesda, MA, USA), leader of the NIH ImageJ project. Financial support was provided by different grants from the following Brazilian agencies: FAPESP (São Paulo Research Foundation), CAPES (Coordination for the Improvement of People with Higher Education), and CNPq (National Council for Scientific and Technological Development).

REFERENCES

- ASTM D5528-13 (2013). Standard test method for mode I interlaminar fracture toughness of unidirectional fiber-reinforced polymer matrix composites. ASTM International, West Conshohocken, PA, www.astm.org, doi: 10.1520/D5528.
- CRAVEN, J.P., BAKER, F.S., THIEL, B.L. & DONALD, A.M. (2002). Consequences of positive ions upon imaging in low vacuum scanning electron microscopy. *J Microsc* **205**, 96–105.
- FORSTER, B., VILLE, D.V., BERENT, J., SAGE, D. & UNSER, M. (2004). Complex wavelets for extended depth-of-field: A new method for the fusion of multichannel microscopy images. *Microsc Res Tech* **65**, 33–42.
- GREENHALGH, E.S. (2009). *Failure Analysis and Fractography of Polymer Composites*. Cambridge: Woodhead Publishing. 595 pp.
- HEIN, L.R.O., CAMPOS, K.A. & CALTABIANO, P.C.R.O. (2012a). Low voltage and variable-pressure scanning electron microscopy of fractured composites. *Micron* **43**, 1039–1049.
- HEIN, L.R.O., OLIVEIRA, J.A. & CAMPOS, K.A. (2013a). Correlative fractography: Combining scanning electron microscopy and light microscopes for qualitative and quantitative analysis of fracture surfaces. *Microsc Microanal* **19**, 496–500.
- HEIN, L.R.O., OLIVEIRA, J.A. & CAMPOS, K.A. (2013b). Correlative light-electron fractography for fatigue striations characterization in metallic alloys. *Microsc Res Tech* **76**, 909–913.
- HEIN, L.R.O., CAMPOS, K.A., CALTABIANO, P.C.R.O. & KOSTOV, K.G. (2013c). A brief discussion about image quality and SEM methods for quantitative fractography of polymer composites. *Scanning* **35**, 196–204.
- HEIN, L.R.O., OLIVEIRA, J.A., CAMPOS, K.A. & CALTABIANO, P.C.R.O. (2012b). Extended depth from focus reconstruction using NIH ImageJ plug-ins: Quality and resolution of elevation maps. *Microsc Res Tech* **75**, 1593–1607.
- HULL, D. (1999). *Fractography: Observing, Measuring, and Interpreting Fracture Surface, Topography*. Cambridge: Cambridge University Press. 366 pp.
- HULL, D. & CLYNE, T.W. (1996). *An Introduction to Composite Materials*. Cambridge: Cambridge University.
- JOY, D.C. (2002). SMART—a program to measure SEM resolution and imaging performance. *J Microsc* **208**, 24–34.
- PALUSZYŃSKI, J. & SŁÓWKO, W. (2009). Measurements of the surface microroughness with the scanning electron microscope. *J Microsc* **233**, 10–17.
- POTTER, R.T. & PURSLOW, D. (1983). The environmental degradation of notched CFRP in compression. *Composites* **14**, 206–225.
- PURSLOW, D. (1981). Some fundamental aspects of composites fractography. *Composites* **12**, 241–247.
- PURSLOW, D. (1984). Composites fractography without an SEM—the failure analysis of a CFRP I-beam. *Composites* **15**, 43–48.
- PURSLOW, D. (1986). Matrix fractography of fibre-reinforced epoxy composites. *Composites* **17**, 289–303.
- PURSLOW, D. (1987a). Matrix fractography of fibre-reinforced thermoplastics, part 1: Peel failures. *Composites* **18**, 365–374.
- PURSLOW, D. (1987b). Further fractographic characteristics of peel failures in CFRP. *Composites* **18**, 255–256.
- PURSLOW, D. (1988a). Matrix fractography of fibre-reinforced thermoplastics, part 2: Shear failures. *Composites* **19**, 115–126.
- PURSLOW, D. (1988b). Fractography of fibre-reinforced thermoplastics, part 3: Tensile, compressive and flexural failures. *Composites* **19**, 358–366.
- PURSLOW, D. & POTTER, R.T. (1984). The effect of environment on the compression strength of notched CFRP—a fractographic investigation. *Composites* **15**, 112–120.
- RASBAND, W.S. (2015). ImageJ, 1997–2014. Bethesda, MD, USA: US National Institutes of Health. Available at <http://imagej.nih.gov/ij>.
- SAWYER, L.C., GRUBB, D.T. & MEYERS, G.F. (2008). *Polymer Microscopy*, 3rd ed New York, NY: Springer. 540 pp.
- VALDECASAS, A.G., MARSHALL, D., BECERRA, J.M. & TERRERO, J.J. (2001). On the extended depth of focus algorithms for brightfield microscopy. *Micron* **32**, 559–569.